Jurnal Elektronika dan Telekomunikasi (JET), Vol. 25, No. 1, August 2025, pp. 38-45
Accredited by KEMDIKBUDRISTEK, Decree No: **158/E/KPT/2021**
doi: 10.55981/jet.704

A Robust SMO-PLL Estimation Algorithm for Enhancing Rotor Position Accuracy and Reducing Chattering Issues in Sensorless FOC of SPMSM

Nektar Cahayasabda*, Sekhul Ishak, Danang Suryo Wibowo, Aulia Rahmah Salsabila, Syifa Fajry Az Zahra, Isyatul Hani'ah, Khoirudin Fathoni, Mario Norman Syah

Department of Electrical Engineering
Faculty of Engineering
Universitas Negeri Semarang
Semarang, Indonesia, 50229

Abstract

Recent advancements in sensorless Field-oriented Control (FOC) of Surface Permanent Magnet Synchronous Motors (SPMSMs) have improved system reliability and cost-effectiveness. However, limitations such as speed chattering and inaccurate rotor position estimation remain problematic for Electric Vehicle (EV) applications. This study developed a sliding mode observer-phase locked loop (SMO-PLL) algorithm applied to sensorless FOC in SPMSMs. The SMO predicts the back EMF of the SPMSM, which the PLL then uses for precise rotor position and speed estimation. Simulations conducted in MATLAB Simulink demonstrate that the SMO-PLL significantly reduces chattering and achieves a rotor position estimation error of only 1 rad/min. While the quantitative integral error criteria for SMO-PLL (IAE: 0.0868, ITAE: 0.3069, ISE: 0.0229, ITSE: 0.0834) are slightly higher than those of Field Observer (FO) and Extended Electromagnetic Field Observer (EEMFO), speed control analysis confirms that SMO-PLL delivers a rapid steady-state response with minimal overshoot and oscillation. These findings are crucial for applications where speed stability is essential for passenger comfort and safety, highlighting the SMO-PLL's potential as a robust sensorless control solution for future EVs.

Keywords: Sliding Mode Observer, SPMSM, Phase Locked Loop, Field-oriented Control, Rotor Position Estimation, Motor Speed Estimation.

I. INTRODUCTION

Surface Permanent Magnet Synchronous Motors (SPMSM) are extensively employed in electric vehicles (EVs) [1], due to their lightweight and compact, highly efficient, reliable, easy to control, and wide speed range characteristics [2]. However, the intrinsic nonlinearity, multi-coupling, and time-varying features of SPMSM necessitate sophisticated control approaches for maximum performance [3]. With recent advancements in microcontroller technology, it has become possible to utilise cost-effective, high-performance digital processors to implement sophisticated sensorless algorithms [4].

Field-oriented control (FOC) is extensively employed in controlling SPMSM due to its effectiveness in various applications. FOC facilitates torque and flux control decoupling, enhancing dynamic performance and ensuring smooth operational characteristics [5]. However, accurate motor speed and rotor position values are crucial to effectively controlling SPMSM through FOC. Traditionally, these values have been measured utilising mechanical sensors such as hall sensors, photoelectric encoders, and rotational transformers to calculate speed and rotor position in electric systems. This increases hardware costs and potentially affects the reliability of SPMSM [6], [7]. Sensorless control methods, such as the injection of high-frequency signals, effectively address these issues, particularly at zero and slow speeds [3], [8], [9].

The advancement of sensorless control technology for SPMSM has become quite popular over the past few years. The advancement of sensorless control methods is classified into medium and high-speed categories, such as direct estimation systems, Model Adaptive Reference Systems (MRAS) [10], extended Kalman filters [11], [12], and low-speed strategies like high-frequency signal injection [3], [8], [9]. However, these methods require enhancement regarding the resistance towards noise, disturbance and computational complexity, resulting in errors and reduced system performance. In contrast, the Sliding Mode Observer (SMO) provides simplicity, high robustness, high resilience towards noise and disturbance, and further high system stability because of the direct control algorithm [13]. Furthermore, despite the introduction of chattering due to switching characteristics along the sliding surface that potentially generate position error and harmonic components in the estimated Back EMF [14], [15], SMO is a proper choice for enhancing SPMSM performance [16]– [18]. These problems can be minimised through careful control design of the SMO algorithm [19].

* Corresponding Author.
Email: nektarcahayasabda@gmail.com
Received: November 25, 2024 ; Revised : July 07, 2025
Accepted: August 06, 2025 ; Published: August 31, 2025

Passive sensorless approaches have received interest because of their ability to avoid extra losses and current distortion [20]. Among that, the study of SMO for estimating rotor position and speed is widespread [21], [22]. However, various methods are proposed to correct the position error resulting from harmonic components in back-EMF estimation [23]–[26]. For instance, [23] shows that improving the actual voltage of the inverter against the reference voltage can improve the control precision and stability of sensorless SPMSM. However, deciding the current polarity at high loads has become even more troublesome, which is necessary for arriving at compensation voltage [25]. Modelling of spatial harmonics has been established for the model-oriented sensorless control methods [26]. However, these model-based strategies involve an offline commissioning process, complicating the implementation. The PLL for the adaptive compensation method based on two synchronous frequency extract filters (SFFs) was proposed in [27]. This method performed better than the adaptive notch filter (ANF), which is highly robust and reduces chattering issues. Unfortunately, SFFs are not suitable for motors with high start-stop frequencies and motor speed changes at one time; the SFF method is not suitable for application to BEVs but is more suitable for motor applications on compressors or blowers with operating speeds that tend to be constant.

The arctangent calculation method derived from the estimated orthogonal back-EMF is the most prevalent technique for extracting rotor position angle information [27]. Consequently, the division operation involved in arctangent calculation can amplify the estimation error. In recent studies, the PLL technique has gained popularity across various applications, including motor control, due to its resilience to disturbances and ability to provide quick and accurate synchronisation information [28]–[30]. However, harmonic components in the input signal for the PLL can reduce PLL bandwidth, adversely affecting the transient response [31]. Each of these contributions enhances the reliability and efficacy of SMO-based sensorless SPMSM control. Unfortunately, these optimisation techniques still produce high back EMF chattering and speed oscillation, notably within high voltage and high current Battery Electric Vehicle (BEV) systems.

Those methods are widely proposed and tested for SPMSM. However, they are not yet simulated and modelled for BEV application. This study developed a high-performance sensorless FOC based on an SMO-PLL estimation algorithm to address the need for high rotor prediction accuracy and minimise speed chattering issues for SPMSM in BEV. The SMO is developed as an observer based on the SPMSM current equation in the $\alpha\beta$ reference frame to extract the motor's back EMF. Despite the low-pass filter that potentially introduces the phase delay, this study developed a PLL to act as a low-pass filter, avoiding the phase delay, eliminating the back-EMF chattering issue, and further improving the rotor position estimation. The SMO-PLL simulation result is compared with the Field Observer (FO) [31], and Extended Electromagnetic Field Observer (EEMFO) [32].

II. PROPOSED SMO-PLL METHOD

The SMO-PLL algorithm utilises the estimated back EMF value at the alpha and beta coordinates to achieve precise rotor position and rotor angular speed value without needing physical sensors. As shown in Figure 1, the controller does not need the position feedback from the motor; it only needs the current data from phase a i_a and phase b i_b. The power electronic topology used in this work is a six-step inverter with six switching devices, as depicted in Figure 2.

The overall system is depicted in Figure 3. It employs cascaded control loops, where an outer speed controller generates current references for inner dq-axis current controllers. Then, SMO estimates the motor's back-EMF, and PLL is then used to derive the rotor's estimated position and speed, enabling the necessary coordinate transformations without physical sensors. Figure 4 depicts the detailed PLL estimating rotor position and speed based on the estimated back EMF. It will get the rotor's angular position and angular speed without requiring physical sensors.

This section comprises four subsystems: the first subsection comprises the SPMSM mathematical model at $\alpha\beta$ coordinate, the second subsystem comprises modelling of the back EMF estimator using SMO, the third section comprises PLL design to estimate rotor angle and speed based on back EMF estimated by SMO, and the fourth sub-sections comprise how the proposed sensorless algorithm is integrated into the FOC method.

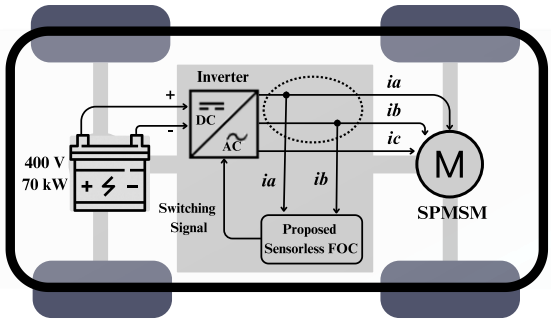

Figure 1. Block diagram of the SMO-PLL method in BEV architecture.

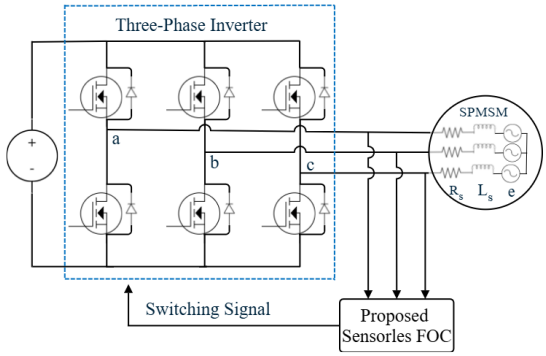

Figure 2. Electrical schematic of SMO-based SPMSM BEV drive system.

A. SPMSM Mathematical Drive Model

Figure 2 shows that SPMSM comprises R, L, and unknown back EMF elements based on that, voltage state equation of SPMSM in the $\alpha\beta$ coordinate system is obtained as (1) [33],

$$\begin{cases} u_\alpha = R_s i_a + \dfrac{d\psi_\alpha}{dt}, \\ u_\beta = R_s i_\beta + \dfrac{d\psi_\beta}{dt}, \end{cases} \tag{1}$$

where $[u_\alpha u_\beta]$ is the stator voltage, R_s is the stator resistance, $[i_\alpha\ i_\beta]$ is the stator current, $[\psi_\alpha\ \psi_\beta]$ is the permanent magnet flux linkage in the $\alpha\beta$ axes, respectively.

The flux linkage equation is as (2),

$$\begin{cases} \psi_\alpha = L_s i_a + \psi_f \cos\theta, \\ \psi_\beta = L_s i_\beta + \psi_f \sin\theta, \end{cases} \tag{2}$$

where the stator winding inductance of SPMSM ($L_\alpha = L_\beta = L_s$), ψ_f is the permanent magnet rotor flux, and θ is the rotor position.

By subtracting (1) and (2), the voltage equation is obtained as (3),

$$\begin{cases} u_\alpha = R_s i_a + L_s \dfrac{di_\alpha}{dt} - \omega\psi_f \sin\theta, \\ u_\beta = R_s i_\beta + L_s \dfrac{di_\beta}{dt} - \omega\psi_f \cos\theta, \end{cases} \tag{3}$$

where ω is the electrical rotor angular speed that can be obtained by differentiating the θ. The state equation of stator current can be obtained by arranging (3) as (4):

$$\begin{cases} \dfrac{di_\alpha}{dt} = \dfrac{1}{L}u_\alpha + \dfrac{1}{L}\omega\psi_f \sin\theta - \dfrac{R_s}{L}i_\alpha, \\ \dfrac{di_\beta}{dt} = \dfrac{1}{L}u_\beta + \dfrac{1}{L}\omega\psi_f \cos\theta - \dfrac{R_s}{L}i_\beta. \end{cases} \tag{4}$$

The back EMF at $\alpha\beta$ axes as (5). it is noticed that the equation of back EMF e_α and e_β contains all the information about the rotor position. Therefore, the speed and position information of SPMSM can be calculated by accurately obtaining and deriving the back EMF.

$$\begin{cases} e_\alpha = -\omega\psi_f \sin\theta, \\ e_\beta = \omega\psi_f \cos\theta. \end{cases} \tag{5}$$

B. Design of Applied SMO

The back EMF signal of SPMSM has sine and cosine waveforms, which contain the SPMSM speed, flux linkage, and rotation angle information. Furthermore, (5) shows that the rotation angle of SPMSM is related to the phase of back EMF, and the speed of SPMSM is related to the amplitude of back EMF. It shows that the rotor position and speed can be obtained utilising the back EMF value as (6) and (7), respectively, [34].

$$\theta = -\arctan\frac{e_\alpha}{e_\beta}. \tag{6}$$

$$\omega = \frac{\sqrt{{e_\alpha}^2 + {e_\beta}^2}}{\psi_f}. \tag{7}$$

The operation of the synovial variable structure control system can be distinguished into two principal stages. Initially, the system moves towards the switching surface that intersects with the synovial hyperfunction, where s ≠ 0, enabling a transition from any direction. Subsequently, the system engages with the switching surface and continues along this interface. The synovial variable structure control design also follows a two-stage process. The sliding mode is defined at the first level, guiding the system to reach it. The system maintains its position within the sliding mode at the second level.

The SMO is developed based on the synovial current observer. According to (4), the sliding surface and the signum function are defined in (8) and (9), respectively,

$$s(x) = \tilde{i}, \tag{8}$$

$$sgn(x) = \begin{cases} 1, & x > 0 \\ 0, & x = 0, \\ -1 & x < 0 \end{cases} \tag{9}$$

where $\tilde{i} = \hat{i} - i$ is the observation current error value, $\hat{i} = \left[\hat{i}_\alpha\ \hat{i}_\beta\right]^T$ is the estimated current value and $i = \left[i_\alpha\ i_\beta\right]^T$ is the measured actual current. Substituting (8) and (9) into the current equation of SPMSM in the $\alpha\beta$ reference coordinate system, the SMO is arranged as (10),

$$\begin{cases} \dfrac{d\hat{i}_\alpha}{dt} = \dfrac{1}{L}u_\alpha - \dfrac{R_s}{L}\hat{i}_\alpha - \dfrac{k}{L_s}\ sgn\left(\tilde{i}_\alpha\right), \\ \dfrac{d\hat{i}_\beta}{dt} = \dfrac{1}{L}u_\beta - \dfrac{R_s}{L}\hat{i}_\beta - \dfrac{k}{L_s}sgn\left(\tilde{i}_\beta\right), \end{cases} \tag{10}$$

where $\tilde{i}_\alpha$ and $\tilde{i}_\beta$ are current error values in the $\alpha\beta$ coordinate, respectively, $\tilde{i}_\alpha = \hat{i}_\alpha - i_\alpha$ and $\tilde{i}_\beta = \hat{i}_\beta - i_\beta$. The parameter k representing the switching gain that must satisfy the conditions for the existence and accessibility of sliding mode motion. Failure to meet these conditions will result in the system's inability to achieve sliding mode motion.

By subtracting (4) from (10), the error equation of the current state, as shown in (11):

$$\begin{cases} \dfrac{d\tilde{i}_\alpha}{dt} = -\dfrac{R_s}{L}\tilde{i}_\alpha - \dfrac{k}{L_s}\ sgn\left(\tilde{i}_\alpha\right) + \dfrac{e_\alpha}{L_s}, \\ \dfrac{d\tilde{i}_\beta}{dt} = -\dfrac{R_s}{L}\tilde{i}_\beta - \dfrac{k}{L_s}sgn\left(\tilde{i}_\beta\right) + \dfrac{e_\beta}{L_s}. \end{cases} \tag{11}$$

From (11), it is evident that the unknown back EMF e_α and e_β components influence the characteristics of the error dynamics. By defining $s(x) = \tilde{i} = 0$ as the sliding surface, the error dynamic equation will gradually stabilise if the conditions of (12) are satisfied.

$$s^T\dot{s} = \begin{pmatrix} (\hat{i}_\alpha - i_\alpha)\cdot(\dot{\hat{i}}_\alpha - \dot{i}_\alpha) \\ (\hat{i}_\beta - i_\beta)\cdot(\dot{\hat{i}}_\beta - \dot{i}_\beta) \end{pmatrix} \leq 0. \tag{12}$$

that is (13) for $\hat{i}_\alpha, \hat{i}_\beta > i_\alpha, i_\beta$

$$s^T\dot{s} = \begin{pmatrix} (\hat{i}_\alpha - i_\alpha)\cdot\left(\frac{1}{L_S}(\hat{i}_\alpha - i_\alpha)e_\alpha - k\left(\frac{R_S}{L_S}(\hat{i}_\alpha - i_\alpha)\right)^2\right) \\ (\hat{i}_\beta - i_\beta)\cdot\left(\frac{1}{L_S}(\hat{i}_\beta - i_\beta)e_\alpha - k\left(\frac{R_S}{L_S}(\hat{i}_\beta - i_\beta)\right)^2\right) \end{pmatrix} \quad (13)$$

and (14) for $\hat{i}_\alpha, \hat{i}_\beta < i_\alpha, i_\beta$

$$s^T\dot{s} = \begin{pmatrix} (\hat{i}_\alpha - i_\alpha)\cdot\left(\frac{1}{L_S}(\hat{i}_\alpha - i_\alpha)e_\alpha - k\left(\frac{R_S}{L_S}(\hat{i}_\alpha - i_\alpha)\right)^2\right) \\ (\hat{i}_\beta - i_\beta)\cdot\left(\frac{1}{L_S}(\hat{i}_\beta - i_\beta)e_\alpha - k\left(\frac{R_S}{L_S}(\hat{i}_\beta - i_\beta)\right)^2\right) \end{pmatrix} \quad (14)$$

Therefore, utilising the form of the Lyapunov function in [35], the value of the sliding mode gain k is $k = \max(|e_\alpha||e_\beta|)$ to ensure $s^T\dot{s} \leq 0$. It can be asserted that a sliding motion can indeed be induced, and the error dynamic equation exhibits asymptotic stability under the condition that the parameters are suitably chosen. Ultimately, the estimated back electromotive force (EMF) expression may be reformulated as indicated in equation (15):

$$\begin{cases} \hat{e}_\alpha = k \cdot sgn\,(\tilde{i}_\alpha), \\ \hat{e}_\beta = k \cdot sgn\,(\tilde{i}_\beta). \end{cases} \quad (15)$$

C. Design of Applied PLL

Considering the signum function's discontinuity and the applied SMO high-frequency interference, a high harmonic in the estimated back EMF signal will be introduced. The harmonic of estimated back EMF potentially led to speed chattering phenomena. Therefore, this study designed the PLL to deal with that, as shown in Figure 3. The PLL used the estimated back EMF to calculate the accurate rotor angle and angular speed of SPMSM.

The PLL system functions as a low-pass filter, efficiently removing high-frequency harmonic components from the estimated back EMF. As a result, it provides a highly accurate rotor position estimation signal.

In Figure 3, the DE value is the PI controller input on the PLL as (16) [33]:

$$\Delta e = \hat{\omega}\psi_f \sin(\theta - \hat{\theta}). \quad (16)$$

Furthermore, Figure 3 also shows that at $\theta - \hat{\theta} \to 0$ condition, then $\sin(\theta - \hat{\theta}) \to \theta - \hat{\theta}$ [33]. The DE in (16) can be arranged as (17):

$$\Delta e = \hat{\omega}\psi_f. \quad (17)$$

By recalling the (18) and looking at Figure 3, the estimated rotor speed $\hat{\omega}$ is arranged as (18):

$$\hat{\omega} = \Delta e\psi_f \left(k_p + \frac{k_i}{s}\right) = \frac{\Delta e k_p s + \Delta e k_i}{s^2}. \quad (18)$$

Thus, the estimated angular speed directly utilising the integration of the estimated rotor speed $\hat{\omega}$ as (19):

$$\hat{\theta} = \int \hat{\omega}\, dt. \quad (19)$$

The steady-state error of the PLL from (18) is zero, which means that the control strategy can be realised in the overall SPMSM sensorless system.

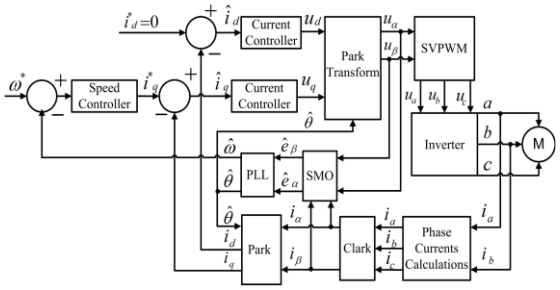

Figure 3. Diagram block of sensorless BEV SPMSM vector control system under SMO.

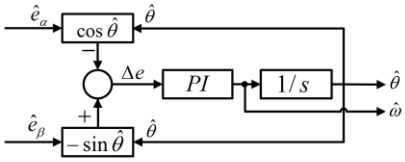

Figure 4. Diagram block of PLL.

D. FOC Design

The detailed proposed FOC sensorless algorithm used for speed control applications is shown in Figure 4. The process starts with Clarke transformation, which transforms a three-phase stator current into two orthogonal vectors. The Park transformation rotates these parts with reference to a spinning frame of reference in the context of rotor flux. Such transformations essentially demodulate the d-axis (current carrying or flux producing) and the q-axis (current carrying or torque producing) current from the stator, thereby affording an individual control of torque and flux.

The speed reference is denoted as ω^*, is compared to the feedback speed determined by the SMO-PLL estimator $\hat{\omega}$. The resulting error is managed using a Proportional-Integral (PI) controller, which generates the i_q^* component. Torque is managed indirectly by adjusting the stator current vector, where i_d^* and i_q^* denote the direct and quadrature axis components of the stator current in the rotating reference frame. Furthermore, $\hat{i}_d$ is maintained at 0, while $\hat{i}_q$ is maximised to achieve optimal torque.

The reference currents are matched with the feedback currents, and the resulting errors are processed by their respective PI controllers. These controllers then generate the reference values u_d and u_q, which are then transformed into u_α and u_β using an inverse Park transformation informed by the position calculated from the SMO-based estimator. Lastly, u_α and u_β are sent to the Space Vector Modulator, which regulates the converter's switching signals.

III. SIMULATION RESULTS AND DISCUSSION

For this study, 400V, 70kW SPMSM is chosen. The overall SPMSM parameters and specifications are obtained by looking at the datasheet and utilised for simulation, depicted in Table 1. Figure 5 shows a simulation developed on the SMO-PLL MATLAB

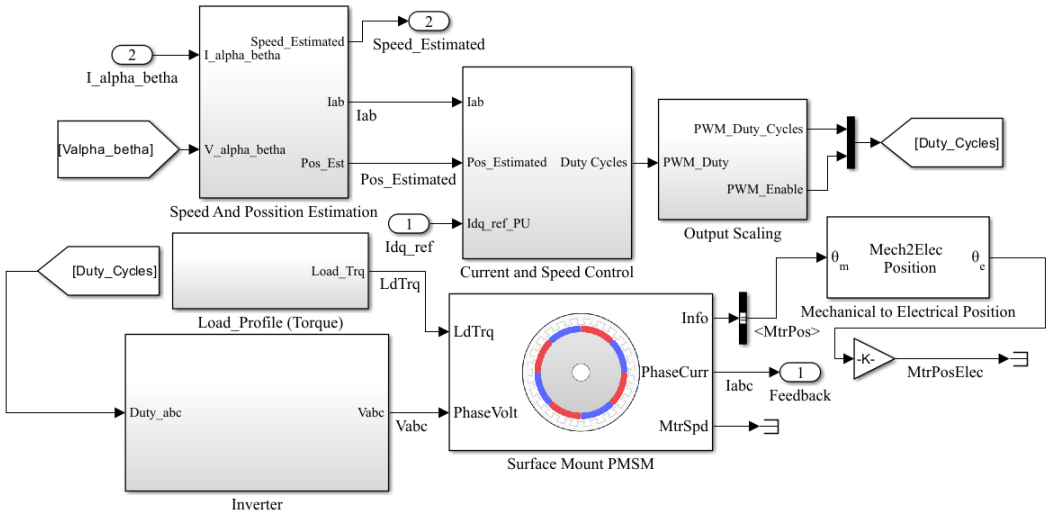

Figure 5. MATLAB Simulink Implementation of SMO-PLL.

TABLE 1
PARAMETERS OF SPMSM

Parameters	Value	Parameters	Value
Rated current	300A	Back EMF constant	0.1 V/krpm
Maximum speed	16000 RPM	Torque Constant	0.1 Nm/A
DC bus voltage	400 V	Rotor Inertia	0.01 kg·m^2
Stator resistance	0.015 Ω	Damping Coefficient	0.0001 N·m·s
DQ-axis inductance	0.0001 H	Permanent Magnet Flux	0.05 Weber

Simulink environment. The motor torque is tuned to its rated torque to obtain maximum torque at different speeds. The simulation was performed in MATLAB Simulink 2024a using the sensorless FOC program as an example, which was then modified to use the SPMSM profile with the current BEV and SMO-PLL estimate technique.

A. Rotor Speed

Figure 6 shows the algorithm performance in the transient response. The SMO-PLL, FO, and EEMFO methods successfully achieved the reference speed. The FO method has the fastest response but has a high overshoot accompanied by the longest speed chattering. The EEMFO method demonstrates the characteristics of a fast response, high overshoot, and speed chattering when a sudden change occurs. Furthermore, the SMO-PLL shows a fast steady-state response accompanied by lower overshoot and speed chattering compared to FO and EEMFO methods.

The robustness of the SMO-PLL estimation algorithm is demonstrated through its consistent performance and stability under dynamic conditions, maintaining high estimation accuracy despite system

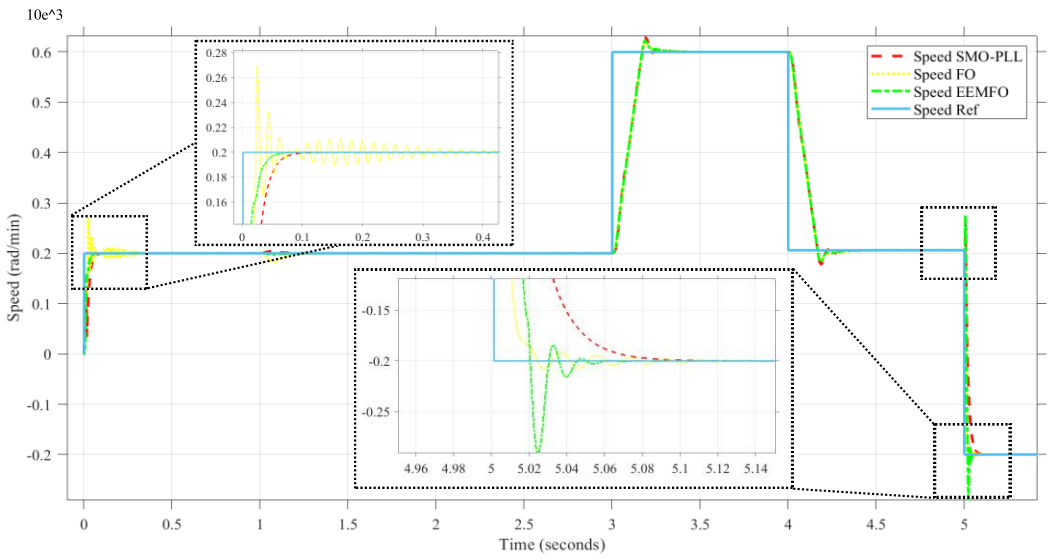

Figure 6. Actual and Reference Speed Under Proposed SMO, FO, and EEMFO.

challenges. In sudden change conditions from a speed of 200 rad/min forward to 200 rad/min reverse, the FO and EEMFO methods experienced high overshoot and speed chattering before the system reached the steady state condition. In contrast, the SMO-PLL method demonstrates superior response characteristics, exhibiting significantly reduced overshoot and diminished speed chattering compared to the FO and EEMFO methods. Furthermore, in Figure 10, the rotor position estimation error remains minimal at 1 rad/min, highlighting the algorithm's accuracy.

Additionally, Table 2 presents a qualitative analysis of speed response, with the performance of the SMO-PLL, FO, and EEMFO methods quantitatively assessed using integral error performance indices: Integral Absolute Error (IAE), Integral Time Absolute Error (ITAE), Integral Squared Error (ISE), and Integral Time Squared Error (ITSE). These metrics comprehensively evaluate the system's capability to track the reference speed and minimise deviations over time. As summarised, the FO method demonstrated the lowest values: IAE (0.0823), ITAE (0.2779), ISE (0.0208), and ITSE (0.0737), closely followed by the EEMFO method. Although the proposed SMO-PLL algorithm showcased impressive qualitative performance, it produced slightly higher values across all indices (IAE: 0.0868, ITAE: 0.3069, ISE: 0.0229, ITSE: 0.0834). This numerical comparison indicates that, in terms of cumulative error minimisation throughout the entire simulation period, the FO and EEMFO methods may be considered superior when assessed solely on these integrated error values.

However, a critical aspect for BEV applications is the overall error magnitude and the quality of the transient response, particularly regarding smoothness and the absence of oscillations. As depicted in Figure 6, despite the slightly higher integral error values, the SMO-PLL method delivers a significantly smoother speed response with minimal overshoot and virtually no chattering or sustained oscillation. Conversely, FO and EEMFO, while achieving lower error integrals, exhibit noticeable overshoot and prolonged speed chattering. In BEV powertrains, even minor speed oscillations can lead to significant issues such as passenger discomfort, increased mechanical stress on components, and reduced drivetrain longevity. Therefore, prioritising a smooth, oscillation-free response, as achieved by the SMO-PLL, is paramount for ensuring the safety, comfort, and long-term reliability of the vehicle, outweighing the numerical advantage of marginally lower integral error metrics in this specific application context. As a result, the FO[31] and EEMFO [32]. Methods are considered less suitable for BEV characteristics due to the overshooting and chattering issues.

TABLE 2
ERROR QUANTITATIVE COMPARISON

Method	IAE	ITAE	ISE	ITSE
Speed SMO PLL	0.0868	0.3069	0.0229	0.0834
Speed FO	0.0823	0.2779	0.0208	0.0737
Speed EEMFO	0.0831	0.2932	0.0224	0.0811

B. SPMSM Current, Voltage, and Switching Signal Characteristics

Figures 7 and 8 show the characteristics of SPMSM stator current and voltage under a sudden speed change. The proposed SMO-PLL algorithm performs with high stability and has a low harmonic current during operation. This can be seen through the three-phase current signal waveform, which has perfect sine characteristics. The three-phase voltage waveform on the SPMSM also possesses perfect sine characteristics. However, as Figures 7 and 8 show, the voltage is ahead of the current by ninety degrees. The current lags due to the inductive nature of the SPMSM, causing inductive reactance, which triggers a delay in current changes. Meanwhile, Figure 9 depicts the switching characteristics of the inverter using Space Vector PWM (SVPWM).

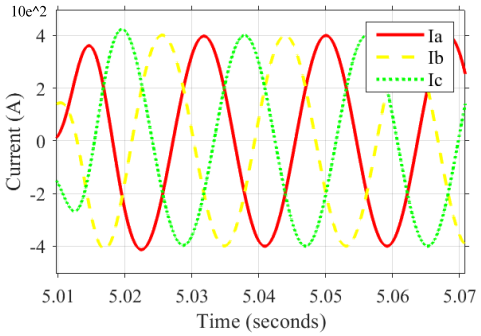

Figure 7. Stator Current of SPMSM

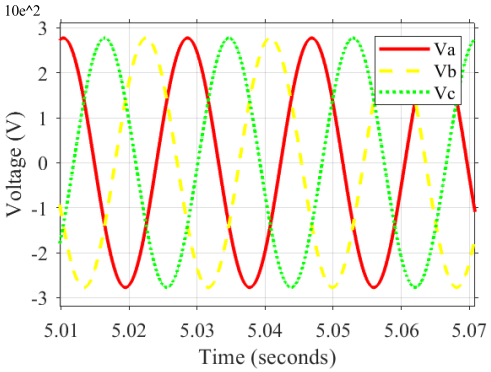

Figure 8. Stator Voltage of SPMSM.

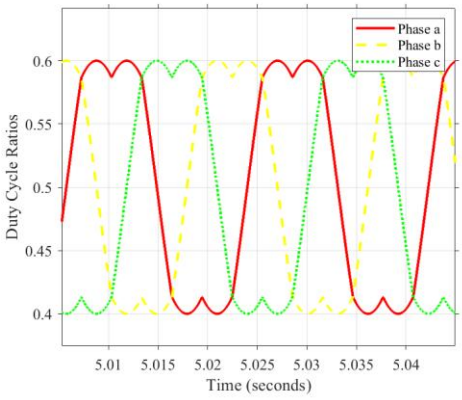

Figure 9. Phase a, b, and c of SVPWM of the Inverter.

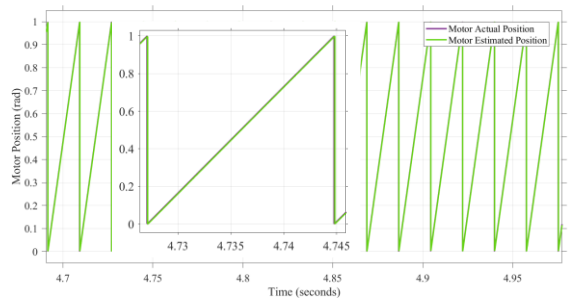

Figure 10. Rotor Position Estimation Under SMO-PLL.

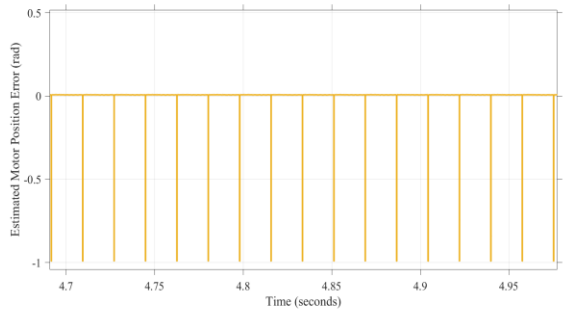

Figure 11. Rotor Position Estimation Error under SMO-PLL.

C. Rotor Position Error

The performance of the proposed SMO-PLL method in estimating the rotor position is depicted in Figure 10. The SMO-PLL performs very well, and, as the rotor position estimation results depicted in Figure 10, there is no instance of chattering. This indicates that the PLL algorithm has effectively mitigated the chattering commonly associated with the sliding mode process. Additionally, the SMO-PLL maintains a consistent phase error and remains in a phase-locked state with no phase lag or amplitude attenuation. The estimated rotor position closely matches the actual angle, which significantly reduces high-frequency noise and harmonics in the back EMF, resulting in stabilised output and enhanced control performance that aligns well with the requirements for PMSM operation.

The rotor position error is the discrepancy between the actual rotor position and the position the proposed SMO-PLL estimates. As depicted in Figure 11, the maximum rotor position estimation error associated with the proposed SMO-PLL is 1 rad/min. This finding substantiates the high accuracy and robustness of the SMO-PLL estimation algorithm, demonstrating its effectiveness in rotor position estimation within the system.

IV. Conclusion

The results of the sensorless FOC simulation based on the SMO-PLL as an algorithm to predict rotor position and motor speed demonstrate a rapid response with minimal speed chattering and overshoot. Regarding speed control, the SMO method outperforms the FO and EEMFO methods, although the EEMFO method still excels in accurately estimating rotor position. Notably, the rotor position error produced by the SMO method is measured at 1 rad/min, which is considered very good and reliable for BEV. Quantitative error analysis revealed slightly higher values for the SMO-PLL compared to the FO and the EEMFO. However, a critical qualitative assessment, particularly evident in Figure 6, demonstrates that the SMO-PLL's speed response is significantly smoother, effectively eliminating the overshoots and prolonged oscillations observed in the FO and EEMFO methods. Despite marginally higher integral error values, this inherent smoothness is paramount for BEV applications, where speed oscillations can compromise passenger comfort, drivetrain integrity, and overall safety. The findings of this study suggest that further research and development should focus on enhancing the sensorless FOC algorithm to achieve greater accuracy and future validation under hardware implementation, ultimately paving the way for higher technological readiness for implementation in BEV.

Declarations

Conflict of Interest

The authors have declared that no competing interests exist.

Credit Authorship Contribution

Nektar Cahayasabda: Methodology, Software, Investigation, Writing - Original Draft, Formal analysis; Sekhul Ishak: Visualization, Validation; Danang Suryo Wibowo: Formal analysis, Investigation; Aulia Rahmah Salsabila: Data Curation, Resources; Syifa Fajry Az Zahra: Formal analysis, Investigation; Isyatul Hani'ah: Visualization, Validation; Khoirudin Fathoni: Conceptualization, Supervision; Mario Norman Syah: Writing - Review & Editing, Project administration.

Funding

The authors received no financial support for this article's research, authorship, and/or publication.

Acknowledgement

We are grateful for the use of institutional resources provided by UEESRG (UNNES Electrical Engineering Students Research Group), Department of Electrical Engineering, Universitas Negeri Semarang, for supporting and facilitating this study.

References

[1] R. Sreejith and B. Singh, "Improved sliding mode observer-based position sensorless finite control set-model predictive control of pmsm drive for electric vehicle," in *India International Conference on Power Electronics, IICPE*, 2018, vol. 2018-December. doi: 10.1109/IICPE.2018.8709544.

[2] I. I. Abdalla, T. Ibrahim, and N. Bin Mohd Nor, "Development and optimization of a moving-magnet tubular linear permanent magnet motor for use in a reciprocating compressor of household refrigerators," *Int J Electr Power Energy Syst.*, vol. 77, pp. 263–270, May 2016, doi: 10.1016/j.ijepes.2015.11.020.

[3] T. C. Lin and Z. Q. Zhu, "Sensorless operation capability of surface-mounted permanent-magnet machine based on high-frequency signal injection methods," *IEEE Trans Ind Appl*, vol. 51, no. 3, pp. 2161–2171, May 2015, doi: 10.1109/TIA.2014.2382762.

[4] H. H. Chou, Y. S. Kung, N. Q. Quynh, and S. Cheng, "Optimized fpga design, verification and implementation of a neuro-fuzzy controller for pmsm drives," *Math Comput Simul*, vol. 90, pp. 28–44, 2013, doi: 10.1016/j.matcom.2012.07.012.

[5] C. Chen, H. Zhou, G. Wang, and G. Liu, "Unified decoupling vector control of five-phase permanent-magnet motor with

double-phase faults," *IEEE Access*, vol. 8, 2020, doi: 10.1109/ACCESS.2020.3017541.

[6] J. Hu, J. Zou, F. Xu, Y. Li, and Y. Fu, "An improved pmsm rotor position sensor based on linear hall sensors," *IEEE Trans Magn*, vol. 48, no. 11, pp. 3591–3594, 2012, doi: 10.1109/TMAG.2012.2202279.

[7] S. Y. Kim, C. Choi, K. Lee, and W. Lee, "An improved rotor position estimation with vector-tracking observer in pmsm drives with low-resolution hall-effect sensors," *EEE Trans. Ind. Electron.*, vol. 58, no. 9, pp. 4078–4086, Sep. 2011, doi: 10.1109/TIE.2010.2098367.

[8] W. C. Chi and M. Y. Cheng, "Implementation of a sliding-mode-based position sensorless drive for high-speed micro permanent-magnet synchronous motors," *ISA Trans*, vol. 53, no. 2, pp. 444–453, 2014, doi: 10.1016/j.isatra.2013.09.017.

[9] X. Song, B. Han, S. Zheng, and S. Chen, "A novel sensorless rotor position detection method for high-speed surface pm motors in a wide speed range," *IEEE Trans. Power Electron.*, vol. 33, no. 8, pp. 7083–7093, Aug. 2018, doi: 10.1109/TPEL.2017.2753289.

[10] O. C. Kivanc and S. B. Ozturk, "Sensorless pmsm drive based on stator feedforward voltage estimation improved with mras multiparameter estimation," *IEEE/ASME Trans. Mechatron.*, vol. 23, no. 3, 2018, doi: 10.1109/TMECH.2018.2817246.

[11] N. K. Quang, N. T. Hieu, and Q. P. Ha, "FPGA-based sensorless pmsm speed control using reduced-order extended kalman filters," *IEEE Trans. Ind. Electron*, vol. 61, no. 12, pp. 6574–6582, Dec. 2014, doi: 10.1109/TIE.2014.2320215.

[12] Z. Wang, Y. Zheng, Z. Zou, and M. Cheng, "Position sensorless control of interleaved csi fed pmsm drive with extended kalman filter," *IEEE Trans. Magn.*, vol. 48, no. 11, pp. 3688–3691, 2012, doi: 10.1109/TMAG.2012.2197180.

[13] J. Rivera Dominguez, A. Navarrete, M. A. Meza, A. G. Loukianov, and J. Canedo, "Digital sliding-mode sensorless control for surface-mounted pmsm," *IEEE Trans. Industr. Inform.*, vol. 10, no. 1, pp. 137–151, 2014, doi: 10.1109/TII.2013.2262280.

[14] Y. Zhao, W. Qiao, and L. Wu, "An adaptive quasi-sliding-mode rotor position observer-based sensorless control for interior permanent magnet synchronous machines," *IEEE Trans. Power Electron.*, vol. 28, no. 12, 2013, doi: 10.1109/TPEL.2013.2246871.

[15] L. Sun, X. Zhang, L. Sun, and K. Zhao, "Nonlinear speed control for pmsm system using sliding-mode control and disturbance compensation techniques," *IEEE Trans. Power Electron*, vol. 28, no. 3, 2013, doi: 10.1109/TPEL.2012.2206610.

[16] S. Po-Ngam and S. Sangwongwanich, "Stability and dynamic performance improvement of adaptive full-order observers for sensorless pmsm drive," *IEEE Trans. Power Electron*, vol. 27, no. 2, 2012, doi: 10.1109/TPEL.2011.2153212.

[17] M. L. Corradini, G. Ippoliti, S. Longhi, and G. Orlando, "A quasi-sliding mode approach for robust control and speed estimation of pm synchronous motors," *IEEE Trans. Ind. Electron.*, vol. 59, no. 2, 2012, doi: 10.1109/TIE.2011.2158035.

[18] G. Wang, R. Yang, and D. Xu, "DSP-based control of sensorless ipmsm drives for wide-speed-range operation," *IEEE Trans. Ind. Electron.*, vol. 60, no. 2, 2013, doi: 10.1109/TIE.2012.2205360.

[19] D. Liang, J. Li, and R. Qu, "Sensorless control of permanent magnet synchronous machine based on second-order sliding-mode observer with online resistance estimation," *IEEE Trans. Ind. Appl*, vol. 53, no. 4, pp. 3672–3682, Jul. 2017, doi: 10.1109/TIA.2017.2690218.

[20] B. Alessandro *et al.*, "Surface permanent magnet synchronous motors' passive sensorless contro l: a review," *Energies (Basel)*, doi: 10.3390/en15207747.

[21] Z. Yujiao, Y. Haisheng, and W. Shixian, "An improved super-twisting high-order sliding mode observer for sensor less control of permanent magnet synchronous motor," *Energies (Basel)*, doi: 10.3390/en14196047.

[22] Y. Yongjie and L. Xudong, "A novel nonsingular terminal sliding mode observer-based sensorless co ntrol for electrical drive system," *Mathematics*, doi: 10.3390/math10173123.

[23] Y. Park and S. K. Sul, "A novel method utilising trapezoidal voltage to compensate for inverter nonlinearity," *IEEE Trans. Power Electron.*, vol. 27, no. 12, 2012, doi: 10.1109/TPEL.2012.2192451.

[24] Y. Inoue, K. Yamada, S. Morimoto, and M. Sanada, "Effectiveness of voltage error compensation and parameter identification for model-based sensorless control of ipmsm," *IEEE Trans. Ind. Appl.*, vol. 45, no. 1, 2009, doi: 10.1109/TIA.2008.2009617.

[25] T. Hoshino and J. I. Itoh, "Output voltage correction for a voltage source type inverter of an induction motor drive," *IEEE Trans. Power Electron.*, vol. 25, no. 9, 2010, doi: 10.1109/TPEL.2010.2049031.

[26] S. H. Jung, H. Kobayashi, S. Doki, and S. Okuma, "An improvement of sensorless control performance by a mathematical modelling method of spatial harmonics for a synrm," in *The 2010 International Power Electronics Conference - ECCE ASIA*, Sapporo, Japan, pp. 2010-2015, 2010. doi: 10.1109/IPEC.2010.5543555.

[27] R. Wegener, F. Senicar, C. Junge, and S. Soter, "Low cost position sensor for permanent magnet linear drive," in *2007 7th International Conference on Power Electronics and Drive Systems*, Bangkok, Thailand, pp. 1367-1371, 2007. doi: 10.1109/PEDS.2007.4487882.

[28] L. Tong *et al.*, "An srf-pll-based sensorless vector control using the predictive deadbeat algorithm for the direct-driven permanent magnet synchronous generator," *IEEE Trans. Power Electron.*, vol. 29, no. 6, 2014, doi: 10.1109/TPEL.2013.2272465.

[29] T. V. Tran, T. W. Chun, H. H. Lee, H. G. Kim, and E. C. Nho, "PLL-based seamless transfer control between grid-connected and islanding modes in grid-connected inverters," *IEEE Trans. Power Electron.*, vol. 29, no. 10, 2014, doi: 10.1109/TPEL.2013.2290059.

[30] L. Wang, Q. Jiang, L. Hong, C. Zhang, and Y. Wei, "A novel phase-locked loop based on frequency detector and initial phase angle detector," *IEEE Trans. Power Electron.*, vol. 28, no. 10, 2013, doi: 10.1109/TPEL.2012.2236848.

[31] L. Harnefors and H. P. Nee, "A general algorithm for speed and position estimation of ac motors," *Int. J. Appl. Electromagn. Mech*. 2014;45(1-4):845-850.

[32] L. An, D. Franck, and K. Hameyer, "Sensorless field-oriented control using back-emf and flux observer for a surface mounted permanent magnet synchronous motor." in *2015 12th International Computer Conference on Wavelet Active Media Technology and Information Processing (ICCWAMTIP)*. IEEE, 2015.

[33] X. Liu *et al.*, "SMO-based sensorless control of a permanent magnet synchronous motor," *Front Energy Res.*, vol. 10, Feb. 2022, doi: 10.3389/fenrg.2022.839329.

[34] H. Ding, X. Zou, and J. Li, "Sensorless control strategy of permanent magnet synchronous motor based on fuzzy sliding mode observer," *IEEE Access*, vol. 10, pp. 36743–36752, 2022, doi: 10.1109/ACCESS.2022.3164519.

[35] W. Xu, S. Qu, L. Zhao, and H. Zhang, "An improved adaptive sliding mode observer for middle- and high-speed rotor tracking," *IEEE Trans. Power Electron.*, vol. 36, no. 1, pp. 1043–1053, Jan. 2021, doi: 10.1109/TPEL.2020.3000785.